Preprints of the 21st IFAC World Congress (Virtual)
Berlin, Germany, July 12-17, 2020

Velocity Estimation and Robust Non-linear Path Following Control of Autonomous Surface Vehicles ⋆

Guillermo Bejarano * **Sufiyan N-Yo** *,**

* *Departamento de Ingeniería, Escuela Técnica Superior de Ingeniería, Universidad Loyola Andalucía, Sevilla, España (e-mail: gbejarano@uloyola.es).*
** *ETEA-Instituto de Desarrollo, Universidad Loyola Andalucía, Córdoba, España (e-mail: sufiyanyo@uloyola.es)*

Abstract: This work addresses the problem of non-linear path following control for under-actuated autonomous surface vehicles in the horizontal plane. The presence of multiple unknowns is considered, including unmodelled hydrodynamics, internal parametric model uncertainties, and unmeasurable disturbances due to wind, waves, and ocean currents, whereas the surge, sway, and yaw velocities are also considered to be unmeasured. Firstly, a non-linear extended state observer is applied to recover the unmeasured velocities and estimate the lumped generalised disturbances, that include all unknown terms previously detailed. Secondly, regarding the path following control, a surge-guided line-of-sight guidance law is applied to simultaneously compute the surge and heading/yaw references, while a simplified robust-adaptive backstepping control strategy is proposed. The effectiveness and robustness of the proposed estimation and control strategy is verified in simulation considering challenging disturbance and current profiles.

Keywords: System state estimation, Guidance systems, Path following, Robust control, Disturbance rejection, Autonomous vehicles, Marine systems

1. INTRODUCTION

The development of advanced autonomous surface vehicles (ASVs) has recently drawn growing attention due to their broad potential applications. Namely, ASVs allow to access to otherwise unreachable regions and simplify data acquisition by reducing costs and human risk. Environmental monitoring, border surveillance, and other maritime civilian/military applications are envisioned (Zhang et al., 2015), and that is why motion control of ASVs has become a research hotspot in recent years (Xia et al., 2019).

There are mainly two approaches for the problem of driving an ASV along a desired course: trajectory tracking and path following control (PFC) (Aguiar et al., 2005). In the first approach the ASV is required to track a time-parametrised trajectory, while in PFC the ASV is only required to converge to the path in a time free parametrisation. In most practical situations PFC is the only feasible solution, mainly due to ocean currents, and that is why this work focuses on this approach.

The kinetics of an ASV present several difficulties such as unmodelled hydrodynamics, internal model uncertainties, and unmeasurable disturbances due to wind, waves, and ocean currents. All these unknown terms cause the control performance to depend largely on the estimation and cancellation of disturbances. Moreover, regarding affordable ASV implementation, an important task is to recover unmeasured velocities by using only the position-heading information, measured by a global positioning system (GPS) device and a gyrocompass (Liu et al., 2016).

On the one hand, the problem of enhancing the controller robustness in the presence of uncertainties and disturbances has been addressed under different perspectives. Parametric adaptive methods have been applied to estimate unknown parameters (Skjetne et al., 2005), robust control has been proposed to deal with the disturbances (Lekkas and Fossen, 2014), and fuzzy logic systems and neural networks have been applied to handle uncertainties (Chen et al., 2017). However, all these works are based on velocity measurement, which might not be available in low-cost ASVs. On the other hand, Peng et al. (2017) address the simultaneous estimation of unmeasured velocities and uncertainties, but persistent excitation is required. In this work the finite-time convergent non-linear extended state observer (ESO) proposed by Liu et al. (2019) is applied, which allows to estimate simultaneously the unmeasured velocities and the lumped generalised disturbances without persistence of exciting. Moreover, the convergence of the estimation does not depend on the control law.

The PFC approach consists of a guidance module and a control one (Fossen et al., 2003). The first one computes the references on the heading angle and surge velocity, whereas the second one is in charge of driving the actuators to follow the guided references. Regarding the guidance module, the look-ahead-based line of sight (LOS) law has

⋆ The authors would like to acknowledge Spanish AECID (YPACARAI project, reference 2018/ACDE/000773) and Junta de Andalucía (project reference PY18-RE-0009) for funding this work.

Copyright lies with the authors

been traditionally used (Breivik and Fossen, 2005), but it presents some limitations when facing ocean currents and unknown disturbances, thus many improved LOS guidance laws have been proposed in recent years. An integral LOS guidance was first proposed for linear paths by Børhaug et al. (2008) and then extended to curvilinear paths by Lekkas and Fossen (2014). An adaptive LOS guidance was proposed by Fossen et al. (2015) where the sideslip is estimated by an adaptive term, while a compound LOS guidance law was proposed by Miao et al. (2017) based on the time-delay control method and the reduced-order linear ESO technique. However, in these works the surge reference is predefined (usually as a constant value), regardless of the desired path, in such a way that the path following is actually carried out by manipulating the rudder torque, that increases the manoeuvring burden and reduces the overall manoeuvrability. Given this issue, the surge-guided LOS (SGLOS) proposed by Wang et al. (2019) is applied in this work, ensuring that the surge reference is also guided by the path following errors.

Concerning the control module, many methods including deep learning, H_∞, adaptive, sliding mode, backstepping, fuzzy logic, neural network, optimal, and predictive control have been proposed in the literature (Liu et al., 2016). In this work, given the estimation on the lumped generalised disturbances provided by the ESO, a novel simplified robust-adaptive dynamic controller based on backstepping is proposed. This non-linear strategy benefits from the fact that only the inertia matrix of the vessel must be identified, since many non-linear terms of the ASV dynamic model are lumped into the generalised disturbance term. Therefore, the number of hydrodynamic parameters to be identified is reduced, thus the experimental application of this strategy is simplified. Moreover, the proposed dynamic controller turns out to be much simpler than the fuzzy unknown observer-based robust adaptive PFC proposed by Wang et al. (2019), since the number of tuning parameters is much reduced and input-to-state stability can be also ensured. To the authors' knowledge, this is the first work where the disturbance estimation given by the ESO is effectively used within the dynamic controller, thus the latter is the main theoretical contribution of this work.

The remainder of the work is organised as follows. Section 2 presents the ASV model and formulates the control problem. Section 3 presents the proposed strategy, while Section 4 describes the ESO. Section 5 details the SGLOS guidance and the proposed controller, while Section 6 provides some illustrating simulation results. Finally, Section 7 summarises the conclusions and proposes future work.

2. ASV MODELLING AND PFC FORMULATION

2.1 ASV Modelling

The kinematics and dynamics of an ASV moving in a horizontal plane can be modelled as follows (Fossen, 2011):

$$\begin{cases} \dot{\boldsymbol{\eta}} = \boldsymbol{R}(\boldsymbol{\eta})\boldsymbol{\nu} \\ \boldsymbol{M}\dot{\boldsymbol{\nu}} = -\boldsymbol{C}(\boldsymbol{\nu})\boldsymbol{\nu} - \boldsymbol{D}(\boldsymbol{\nu})\boldsymbol{\nu} - \boldsymbol{g}(\boldsymbol{\nu},\boldsymbol{\eta}) + \boldsymbol{\tau_w} + \boldsymbol{\tau}, \end{cases} \quad (1)$$

where $\boldsymbol{\eta} = [x \;\; y \;\; \psi]^T$ is the planar position/heading vector expressed in the earth-fixed inertial frame {n}, $\boldsymbol{\nu} = [u \; v \; r]^T$ is the surge-sway-yaw velocity vector in the body-fixed frame {b}, $\boldsymbol{\tau_w} = [F_{w,u} \; F_{w,v} \; \tau_{w,r}]^T$ refers to the environmental disturbances due to wind, waves, and currents, and $\boldsymbol{\tau} = [F_u \; 0 \; \tau_r]^T$ stands for the force/torque vector to be designed (see Fig. 1). The effect of currents is generally considered at the kinematic level by using relative velocities with respect to the fluid (assumed to be irrotational, Xia et al. (2019)). However, these velocity measurement might not be available, and no observer can provide an estimation for these relative velocities without previous information about currents. Then, to apply the non-linear ESO proposed by Liu et al. (2019), the description of the dynamics in terms of absolute velocities indicated in (1) has been held. The rotation matrix $\boldsymbol{R}(\psi)$ between {b} and {n} is:

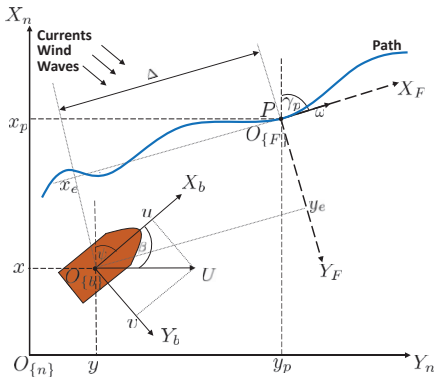

Fig. 1. Path following control geometry

$$\boldsymbol{R}(\psi) = \begin{bmatrix} \cos(\psi) & -\sin(\psi) & 0 \\ \sin(\psi) & \cos(\psi) & 0 \\ 0 & 0 & 1 \end{bmatrix}, \quad (2)$$

while $\boldsymbol{M} = \boldsymbol{M}^T$ is the inertia matrix,the unmodelled hydrodynamics $\boldsymbol{C}(\boldsymbol{\nu})$ is the Coriolis and centrifugal matrix, and $\boldsymbol{D}(\boldsymbol{\nu})$ is the damping matrix, while $\boldsymbol{g}(\boldsymbol{\eta},\boldsymbol{\nu})$ refers to the hydrostatic forces due to buoyancy and unmodelled hydrodynamics. Notice that the dynamic model (1) has three degrees of freedom, while the number of independent control inputs is two (no actuator in the sway direction). Hence, the ASV is a second-order underactuated system.

2.2 PFC Problem Formulation

The reference curvilinear path (see Fig. 1) is considered to be parametrised by a time-dependent variable $\omega(t)$, whose dynamics are also intended to be defined by the guidance module. The Frenet-Serret frame {F} is related to point P, which is a moving point (acting as a virtual target) on the path (Lekkas and Fossen, 2014; Miao et al., 2017; Wang et al., 2019). Then, the axes of {F} are normal and tangent to the desired path at point P. The dynamics of the virtual target represent an extra *design knob* to enhance the PFC. The virtual target velocity u_{tar} is computed as follows:

$$u_{tar} = \sqrt{\dot{x}_p^2 + \dot{y}_p^2} = \dot{\omega}\sqrt{(\partial x_p/\partial\omega)^2 + (\partial y_p/\partial\omega)^2} \quad (3)$$

{F} is rotated with angle γ_p relative to {n}, defined by:

$$\gamma_p = \text{atan2}(\dot{y}_p, \dot{x}_p) = \text{atan2}(\partial y_p/\partial\omega, \partial x_p/\partial\omega), \quad (4)$$

where $\text{atan2}(y,x)$ is the four-quadrant version of the trigonometric function $\arctan(y/x) \in [-\pi/2, \pi/2]$.
The path following errors between the vessel position $(x,$

y) and the virtual target point position (x_p, y_p) can be expressed in {F} as indicated in (5):

$$\begin{bmatrix} x_e \\ y_e \end{bmatrix} \triangleq \boldsymbol{R}^T(\gamma_p) \begin{bmatrix} x - x_p \\ y - y_p \end{bmatrix}, \tag{5}$$

where x_e and y_e are known as the along- and cross-track errors, respectively. The errors dynamics are:

$$\begin{aligned} \dot{x}_e &= U\,\cos(\psi - \gamma_p + \beta) + \dot{\gamma}_p\, y_e - u_{tar}, \\ \dot{y}_e &= U\,\sin(\psi - \gamma_p + \beta) - \dot{\gamma}_p\, x_e, \end{aligned} \tag{6}$$

where $U = \sqrt{u^2 + v^2}$ is the total linear velocity and $\beta = \text{atan2}(v, u)$ is the so-called sideslip angle.

3. ESTIMATION AND CONTROL STRATEGY

A combined estimation and control strategy is proposed in this work. As shown in Fig. 2, a successive control structure is intended, where the controller is divided into 2 subsystems: the kinematic control and the dynamic one.

In the kinematic subsystem, the SGLOS guidance law proposed by Wang et al. (2019) is applied to compute the references on the surge and heading/yaw, in addition to the virtual target velocity, aiming to achieve asymptotic stability of the path following errors. Only the measurement of $\boldsymbol{\eta}$ is needed, which is assumed to be available by using a GPS device and a gyrocompass.The second subsystem addresses the dynamic control, namely the surge and heading/yaw reference tracking, in the presence of highly coupled non-linearities and unknown environmental disturbances. Notice that the presence of currents has been highlighted in Fig. 2, but their influence will be treated as that of external disturbances. Here is where the estimation on the velocities and lumped generalised disturbances provided by the finite-time ESO developed by Liu et al. (2019) comes handy. Given that the ESO makes no assumptions on the control law or on the disturbances, it can be designed regardless of the dynamic controller. The ESO simplifies largely the control law, in such a way that a novel robust-adaptive dynamic controller based on backstepping is proposed in this work. The surge and heading/yaw tracking error convergence to a neighbourhood of zero defined by the upper bound of the estimation error on $\hat{\boldsymbol{\sigma}}$ is theoretically shown.

4. EXTENDED STATE OBSERVER DESIGN

As stated by Liu et al. (2019), from (1), the lumped generalised disturbance vector is defined as shown in (7):

$$\boldsymbol{\sigma} := \boldsymbol{M}^{-1}\left[-\boldsymbol{C}(\boldsymbol{\nu})\boldsymbol{\nu} - \boldsymbol{D}(\boldsymbol{\nu})\boldsymbol{\nu} - \boldsymbol{g}(\boldsymbol{\eta}, \boldsymbol{\nu}) + \boldsymbol{\tau_w}\right]. \tag{7}$$

Then, the system dynamics (1) can be rewritten as:

$$\begin{cases} \dot{\boldsymbol{\eta}} = \boldsymbol{R}(\psi)\,\boldsymbol{\nu}, \\ \dot{\boldsymbol{\nu}} = \boldsymbol{M}^{-1}\boldsymbol{\tau} + \boldsymbol{\sigma}. \end{cases} \tag{8}$$

From (8), Liu et al. (2019) propose the following non-linear ESO with finite-time convergence:

$$\begin{cases} \dot{\hat{\boldsymbol{\eta}}} = \boldsymbol{R}(\psi)\,\hat{\boldsymbol{\nu}} - 3\,\epsilon\,\boldsymbol{R}(\psi)\left[\boldsymbol{R}^T(\psi)\frac{\hat{\boldsymbol{\eta}} - \boldsymbol{\eta}}{\epsilon^2}\right]^{\alpha}, \\ \dot{\hat{\boldsymbol{\nu}}} = \hat{\boldsymbol{\sigma}} + \boldsymbol{M}^{-1}\boldsymbol{\tau} - 3\left[\boldsymbol{R}^T(\psi)\frac{\hat{\boldsymbol{\eta}} - \boldsymbol{\eta}}{\epsilon^2}\right]^{2\alpha-1}, \\ \dot{\hat{\boldsymbol{\sigma}}} = -\frac{1}{\epsilon}\left[\boldsymbol{R}^T(\psi)\frac{\hat{\boldsymbol{\eta}} - \boldsymbol{\eta}}{\epsilon^2}\right]^{3\alpha-2}, \end{cases} \tag{9}$$

where $[\cdot]^{\alpha} = \text{sign}(\cdot)\,|\cdot|^{\alpha}$, while ϵ and α are positive and constant estimation parameters. Notice that only ϵ and α must be tuned. Both the input-to-state stability and finite-time convergence of (9) are shown, provided that Assumption 1 is valid.

Assumption 1. Zhao and Guo (2015); Liu et al. (2019) The lumped generalised disturbance vector $\boldsymbol{\sigma}$ satisfies $\|\dot{\boldsymbol{\sigma}}\| \leqslant \dot{\sigma}^*$, being $\dot{\sigma}^*$ a positive constant.

Then, $\boldsymbol{\nu}$ and $\boldsymbol{\sigma}$ can be estimated by applying (9) from only the measured $\boldsymbol{\eta}$, regardless of the control law. The estimation error could be reduced by decreasing ϵ, but it would make the observer vulnerable to measurement noise. Parameter α allows to achieve finite-time convergence and helps avoiding peaking value problem.

5. GUIDANCE AND DYNAMIC CONTROL LAWS

5.1 Guidance Module

The SGLOS guidance law proposed by Wang et al. (2019) is applied, where the surge reference is:

$$u_{ref} = k_1\,\sqrt{y_e^2 + \Delta^2}, \tag{10}$$

where $k_1 > 0$ is a design parameter and $\Delta > 0$ is the look-ahead distance. Notice that $u_{ref,min} = k_1\,\Delta$, thus k_1 and Δ can be tuned so that the surge reference u_{ref} is always greater than a given desired value.
The heading guidance law is given by (11):

$$\psi_{ref} = \gamma_p - \beta_{ref} - \text{atan}\left(\frac{y_e}{\Delta}\right), \tag{11}$$

where $\beta_{ref} = \text{atan}(v/u_{ref})$. The first term γ_p follows the desired path curvature, the second one β_{ref} compensates the potential sideslip caused by disturbances and currents, while the last one is responsible for driving the cross-track error y_e to zero. The virtual target velocity law is given by:

$$u_{tar} = k_2\,x_e + U_{ref}\,\cos(\psi - \gamma_p + \beta_{ref}), \tag{12}$$

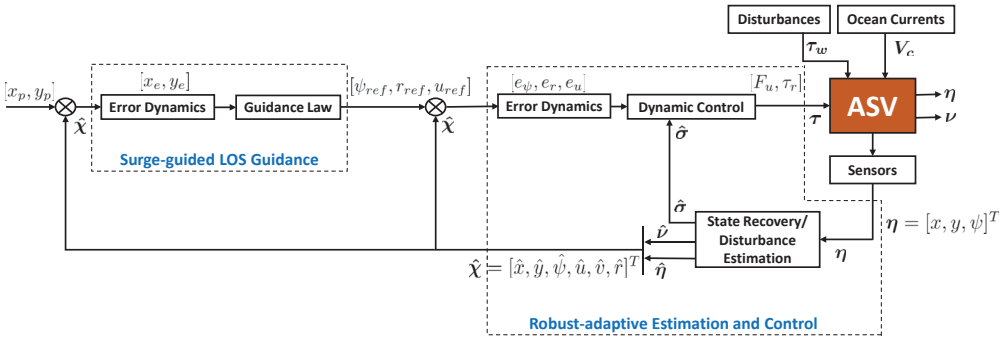

Fig. 2. Proposed estimation and control strategy for PFC of underactuated ASVs

where $k_2 > 0$ is a tuning parameter and $U_{ref} = \sqrt{u_{ref}^2 + v^2}$. Using (10)–(12), the path following errors (5) with dynamics (6) are shown to be globally asymptotically stable (Wang et al., 2019).
Furthermore, given the heading set point (11), a kinematic controller can be designed so that the desired tracking error dynamics (13) are achieved (Miao et al., 2017):

$$e_\psi = \psi - \psi_{ref}, \qquad \dot{e}_\psi = -\, k_\psi\, e_\psi, \tag{13}$$

where $k_\psi > 0$ is a control gain. The virtual command for the yaw dynamic controller is then computed as follows:

$$r_{ref} = \dot{\psi}_{ref} - k_\psi\, (\psi - \psi_{ref}), \tag{14}$$

where low-pass derivative filters are used to compute the successive time derivatives of ψ_{ref}.

5.2 Dynamic Control Design

Regarding the surge dynamic control, the dynamics (8) can be rearranged as follows:

$$\dot{u} = g_{\dot{u}}\, F_u + \sigma_u, \tag{15}$$

where $g_{\dot{u}} = 1/m_{11}$ and σ_u is the first component of $\boldsymbol{\sigma}$. Given the surge reference (10), if the tracking error dynamics indicated in (16) are desired:

$$e_u = u - u_{ref}, \qquad \dot{e}_u = -\, k_u\, e_u, \tag{16}$$

where $k_u > 0$ is a control gain, the following control law is proposed:

$$F_u = \frac{1}{g_{\dot{u}}}\, \left[\dot{u}_{ref} - \hat{\sigma}_u - k_u\, (\hat{u} - u_{ref})\right]. \tag{17}$$

Theorem 1. Under Assumption 1, the proposed control law (17), and the extended disturbance observer (9), the surge tracking error (16) converges to a neighbourhood of zero, defined by the upper bound of the estimation error on the lumped generalised disturbances.

Proof. The finite-time convergence of the estimations $\hat{\boldsymbol{\nu}}$ and $\hat{\boldsymbol{\sigma}}$ is shown in Theorem 4 in Liu et al. (2019), where no assumptions about the control law are made. Specifically, the finite-time convergence of the estimation errors to a region around zero whose amplitude depends on $\dot{\sigma}^*$ is ensured.
Consider the following Lyapunov function:

$$V_u = \frac{1}{2}\, e_u^2 \geqslant 0\,. \tag{18}$$

Differentiating V_u along (16) and (17) produces:

$$\begin{aligned}\dot{V}_u &= e_u \dot{e}_u = e_u(\dot{u} - \dot{u}_{ref}) = e_u(-k_u e_u + \sigma_u - \hat{\sigma}_u) = \\ &= -k_u e_u^2 + e_u e_{\sigma_u} \leqslant -|e_u|(|e_u|k_u - |e_{\sigma_u}|).\end{aligned} \tag{19}$$

According to Liu et al. (2019), the norm of the estimation error on the lumped generalised disturbance $e_{\sigma_u} := \sigma_u - \hat{\sigma}_u$ is bounded and its upper bound turns out to depend on $\dot{\sigma}^*$. Therefore, the norm of e_u is bounded:

$$|e_u| \leqslant \frac{|e_{\sigma_u}|}{k_u}. \tag{20}$$

Concerning the heading/yaw dynamic control, the corresponding dynamics (8) can be expressed as:

$$\dot{r} = g_{\dot{r}}\, \tau_r + \sigma_r, \tag{21}$$

where $g_{\dot{r}} = m_{22}/(m_{22}m_{33} - m_{23}^2)$ and σ_r is the third component of $\boldsymbol{\sigma}$. Given the yaw reference (14), if the yaw tracking error dynamics (22) are desired:

$$e_r = r - r_{ref}, \qquad \dot{e}_r = -\, k_r\, e_r, \tag{22}$$

where $k_r > 0$ is a control gain, the following control law is proposed:

$$\tau_r = \frac{1}{g_{\dot{r}}}\, \left[\ddot{\psi}_{ref} - k_r\, (r - r_{ref}) - k_\psi\, (r - \dot{\psi}_{ref}) - \hat{\sigma}_r\right]. \tag{23}$$

Theorem 2. Under Assumption 1, the proposed control law (23), the virtual reference for the yaw (14), and the extended disturbance observer (9), the heading and yaw tracking errors (13) and (22) converge to a neighbourhood of zero, defined by the upper bound of the estimation error on the lumped generalised disturbances.

Proof. The finite-time convergence of the estimation errors of $\hat{\boldsymbol{\nu}}$ and $\hat{\boldsymbol{\sigma}}$ to a region around zero whose amplitude depends on $\dot{\sigma}^*$ is shown in Theorem 4 by Liu et al. (2019).

Consider the following Lyapunov function:

$$V_{\psi,r} = \frac{1}{2}\, e_\psi^2 + \frac{1}{2}\, e_r^2 \geqslant 0\,. \tag{24}$$

Differentiating $V_{\psi,r}$ along (13), (14), (22), and (23) yields:

$$\begin{aligned}&\dot{V}_{\psi,r} = e_\psi \dot{e}_\psi + e_r \dot{e}_r = e_\psi(r - \dot{\psi}_{ref}) + e_r(g_{\dot{r}}\tau_r + \sigma_r - \dot{r}_{ref}) \\ &= e_\psi(e_r + r_{ref} - \dot{\psi}_{ref}) + e_r\left[\ddot{\psi}_{ref} - k_r(r - r_{ref}) - \right. \\ &\left. - k_\psi(r - \dot{\psi}_{ref}) - \hat{\sigma}_r + \sigma_r - \dot{r}_{ref}\right] = \\ &= e_\psi(e_r + \dot{\psi}_{ref} - k_\psi e_\psi - \dot{\psi}_{ref}) + \\ &+ e_r\left[-k_r(r - r_{ref}) - k_\psi(r - \dot{\psi}_{ref}) + e_{\sigma_r}\right] = \\ &= e_\psi(e_r - k_\psi e_\psi) + e_r\left[-k_r e_r - k_\psi(e_r - k_\psi e_\psi) + e_{\sigma_r}\right] = \\ &= -k_\psi e_\psi^2 - k_r e_r^2 - k_\psi e_r^2 + (1 + k_\psi^2) e_\psi e_r + e_r e_{\sigma_r} = \\ &= -\begin{bmatrix} e_\psi & e_r \end{bmatrix} \begin{bmatrix} k_\psi & -1 \\ -k_\psi^2 & k_\psi + k_r \end{bmatrix} \begin{bmatrix} e_\psi \\ e_r \end{bmatrix} + \begin{bmatrix} e_\psi & e_r \end{bmatrix} \begin{bmatrix} 0 \\ e_{\sigma_r} \end{bmatrix},\end{aligned} \tag{25}$$

where $\dot{r}_{ref}$ is assumed to match $\ddot{\psi}_{ref}$. If the tracking error vector $\boldsymbol{e_{\psi,r}} \equiv [e_\psi\ e_r]^T$ is defined, as well as the control gain matrix $\boldsymbol{K_{\psi,r}} \equiv \begin{bmatrix} k_\psi & -1 \\ -k_\psi^2 & k_\psi + k_r \end{bmatrix}$ and the disturbance error vector $\boldsymbol{G_{\sigma_r}} \equiv [0\ e_{\sigma_r}]^T$, $\dot{V}_{\psi,r}$ yields:

$$\begin{aligned}\dot{V}_{\psi,r} &= -\,\boldsymbol{e}_{\boldsymbol{\psi,r}}^T\, \boldsymbol{K_{\psi,r}}\, \boldsymbol{e_{\psi,r}} + \boldsymbol{e}_{\boldsymbol{\psi,r}}^T\, \boldsymbol{G_{\sigma_r}} \leqslant \\ &\leqslant -\|\boldsymbol{e_{\psi,r}}\|\,(\|\boldsymbol{e_{\psi,r}}\|\|\boldsymbol{K_{\psi,r}}\| - \|\boldsymbol{G_{\sigma_r}}\|)\,.\end{aligned} \tag{26}$$

$\boldsymbol{K_{\psi,r}}$ is positive definite provided that k_ψ and k_r are positive. Since the norm of $e_{\sigma_r} := \sigma_r - \hat{\sigma}_r$ is bounded, the norm of $\boldsymbol{e_{\psi,r}}$ is bounded:

$$\|\boldsymbol{e_{\psi,r}}\| \leqslant \frac{\|\boldsymbol{G_{\sigma_r}}\|}{\|\boldsymbol{K_{\psi,r}}\|} \leqslant \frac{|e_{\sigma_r}|}{\lambda_{min}(\boldsymbol{K_{\psi,r}})}, \tag{27}$$

where $\lambda_{min}(\boldsymbol{K_{\psi,r}})$ is the minimum eigenvalue of $\boldsymbol{K_{\psi,r}}$.

6. SIMULATION RESULTS

Some simulation results are provided to verify the effectiveness and robustness of the proposed strategy. The CyberShip II (a 1:70 scale replica of a supply ship) has been used as the test-bed (Skjetne et al., 2004). The estimation/control parameters have been gathered in Table 1, while the sampling time is set to 0.1 s.

The desired path is the parametrised curve given by (28):

Table 1. Estimation and control parameters

Parameter	Δ	k_1	k_2	k_u	k_ψ	k_r	ϵ	α
Value	8	0.125	2	2	1	4	0.15	1
Units	m	s^{-1}	s^{-1}	s^{-1}	s^{-1}	s^{-1}	s	–

$$\begin{cases} x_p(\omega) = 10\sin(0.1\omega) + \omega \\ y_p(\omega) = \omega, \end{cases} \tag{28}$$

where $\omega(t)$ is the path variable presented in Section 2.2. The initial kinematics and dynamics of the ASV are $\boldsymbol{\eta}(t = 0) = [0\ 10\ 0]^T$ and $\boldsymbol{\nu}(t = 0) = [0\ 0\ 0]^T$. Challenging disturbance profiles have been considered, where the models regarding wind and wave disturbances provided by Fossen (2011) have been applied. The environmental conditions are those of Ypacaraí lake, in Paraguay, where wind of up to 17.5 km/h has been considered and its direction is selected to further disturb the vessel, according to the desired path. Moreover, a linear model for first- and second-order wave-induced forces has been applied, following the JONSWAP spectrum (Hasselmann et al., 1973). Moreover, the vessel model in terms of relative velocities (Xia et al., 2019) is simulated to explicitly consider the irrotational currents $\boldsymbol{V_c} = [V_x\ V_y\ 0]^T$ (expressed in the inertial frame {n}). The current speed and direction have been modelled as first-order Gauss-Markov processes (Fossen, 2011).

Fig. 3 shows the path following under the disturbances and current profiles shown in Fig. 4 and 5, while Fig. 6 shows the along- and cross-track errors. Fig. 7 represents the behaviour of the controlled surge, while Fig. 8 depicts the control actions, where saturation has been considered ($F_u \in [0,\ 2]$ N, $\tau_r \in$ [-1.5, 1.5] N m). Finally, Fig. 9 and Fig. 10 show the performance of the ESO, specifically for the sway velocity v and the yaw-related component of $\boldsymbol{\sigma}$.

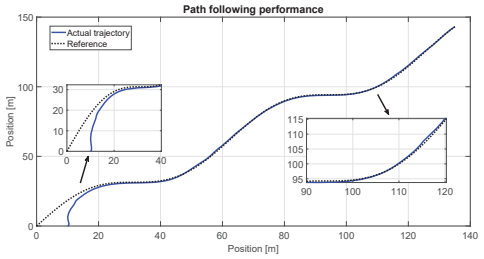

Fig. 3. Path following

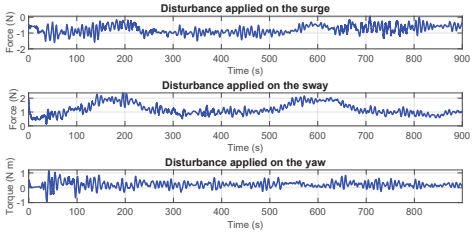

Fig. 4. Wind- and wave-related disturbance profiles

It is shown in Fig. 3 that the proposed strategy achieves remarkable performance and the path following errors shown in Fig. 6 converge smoothly to zero despite the challenging disturbance and current profiles shown in Fig. 4 and 5. The SGLOS guidance parameters have been tuned so that the minimum u_{ref} is 0.15 m s^{-1}, as shown in Fig. 7. Notice in Fig. 8 that, in contrast to the work by Wang et al. (2019), the control actions F_u and τ_r are bounded. Then, the thrust force F_u is shown to be saturated at the beginning , since the surge must be increased from the zero initial condition to the reference provided by the SGLOS guidance law, that turns

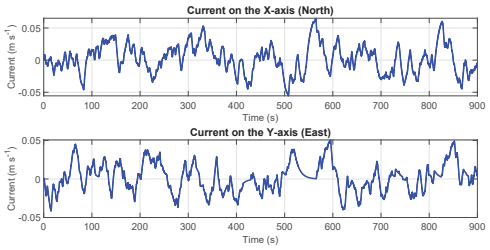

Fig. 5. Current profile expressed in the inertial frame {n}

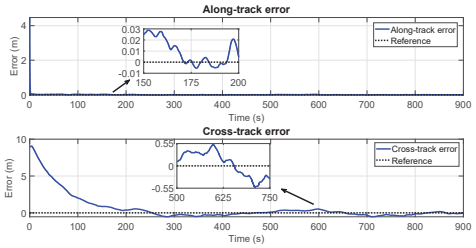

Fig. 6. Along- and cross-track errors

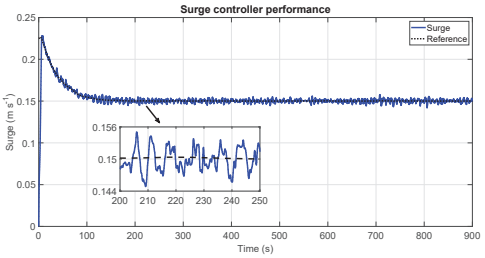

Fig. 7. Surge control

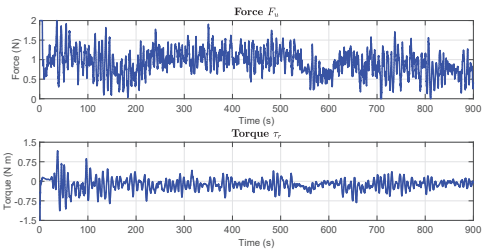

Fig. 8. Control actions

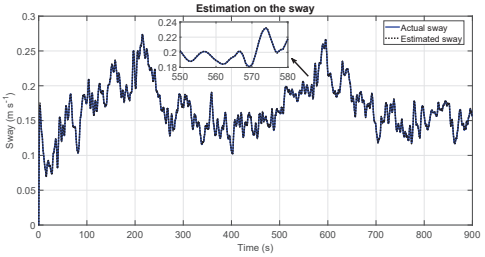

Fig. 9. Sway estimation

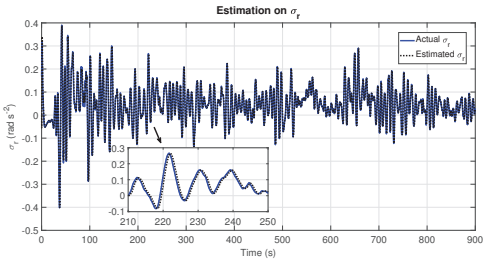

Fig. 10. Yaw-related generalised disturbance estimation

out to be higher than 0.15 m s^{-1} when the cross-track error is significant. Regarding the control parameters, higher values of Δ usually drive to smoother control, while a small Δ implies aggressive steering. Parameter k_1 affects the contribution of the surge reference when the tracking errors are significant, in such a way that the higher k_1, the higher u_{ref} in the case that the cross-track error y_e is not negligible, and thus the higher the initial thrust force. Parameter k_2 defines the velocity with which the along-track error x_e is driven to zero. The control gains k_u, k_ψ, and k_r affect the corresponding reference tracking, thus higher values of these parameters cause the controller to be more aggressive. Concerning state recovery and lumped generalised disturbance estimation, it can be checked in Fig. 9 and 10 that the ESO provides an accurate estimation of $\boldsymbol{\nu}$ and $\boldsymbol{\sigma}$, regardless of the control actions.

7. CONCLUSIONS AND FUTURE WORK

In this work accurate PFC of an ASV subject to multiple disturbances and uncertainties has been achieved by applying a novel estimation and control approach. The ESO allows to accurately recover the unmeasured velocities, as well as estimate the lumped generalised disturbances, and the dynamic control benefits from this estimation to derive a simplified robust-adaptive strategy that makes the path following tracking errors converge to a neighbourhood of zero whose amplitude depends on the estimation error. The SGLOS law provides simultaneous surge and heading guidance, thereby enhancing the overall PFC performance. Simulation results show that the proposed strategy achieves remarkable performance despite being subjected to challenging disturbances and time-varying currents. Future work will consider the influence of input saturation on the dynamic controller, as well as smoother differentiation of the surge and heading references. Moreover, the experimental application of the proposed strategy to a low-cost in-house-designed ASV is intended in the near future.

REFERENCES

Aguiar, A.P., Hespanha, J.P., and Kokotović, P.V. (2005). Path-following for non-minimum phase systems removes performance limitations. *IEEE Trans. Autom. Control*, 50(2), 234–239.

Børhaug, E., Pavlov, A., and Pettersen, K.Y. (2008). Integral LOS control for path following of underactuated marine surface vessels in the presence of constant ocean currents. In *2008 47th IEEE Conf. Decis. Control*, 4984–4991. IEEE.

Breivik, M. and Fossen, T.I. (2005). Guidance-based path following for autonomous underwater vehicles. In *Proc. OCEANS 2005 MTS/IEEE*, 2807–2814. IEEE.

Chen, M., Chen, S.D., and Wu, Q.X. (2017). Sliding mode disturbance observer-based adaptive control for uncertain MIMO nonlinear systems with dead-zone. *Int. J. Adapt. Control Signal Process.*, 31(7), 1003–1018.

Fossen, T.I., Pettersen, K.Y., and Galeazzi, R. (2015). Line-of-sight path following for Dubins paths with adaptive sideslip compensation of drift forces. *IEEE Trans. Control Syst. Technol.*, 23(2), 820–827.

Fossen, T.I. (2011). *Handbook of marine craft hydrodynamics and motion control*. John Wiley & Sons, United Kingdom.

Fossen, T.I., Breivik, M., and Skjetne, R. (2003). Line-of-sight path following of underactuated marine craft. In *6th IFAC Conf. Manoeuvring Control Mar. Craft*, 211–216.

Hasselmann, K., Barnett, T., Bouws, E., Carlson, H., Cartwright, D., Enke, K., Ewing, J., Gienapp, H., Hasselmann, D., Kruseman, P., et al. (1973). Measurements of wind-wave growth and swell decay during the Joint North Sea Wave Project (JONSWAP). *Ergänzungsheft 8-12*.

Lekkas, A.M. and Fossen, T.I. (2014). Integral LOS path following for curved paths based on a monotone cubic hermite spline parametrization. *IEEE Trans. Control Syst. Technol.*, 22(6), 2287–2301.

Liu, L., Wang, D., and Peng, Z. (2019). State recovery and disturbance estimation of unmanned surface vehicles based on nonlinear extended state observers. *Ocean Eng.*, 171, 625–632.

Liu, Z., Zhang, Y., Yu, X., and Yuan, C. (2016). Unmanned surface vehicles: An overview of developments and challenges. *Annu. Rev. Control*, 41, 71 – 93.

Miao, J., Wang, S., Tomovic, M.M., and Zhao, Z. (2017). Compound line-of-sight nonlinear path following control of underactuated marine vehicles exposed to wind, waves, and ocean currents. *Nonlinear Dyn.*, 89(4), 2441–2459.

Peng, Z., Wang, J., and Wang, D. (2017). Distributed containment maneuvering of multiple marine vessels via neurodynamics-based output feedback. *IEEE Trans. Ind. Electron.*, 64(5), 3831–3839.

Skjetne, R., Fossen, T.I., and Kokotović, P.V. (2005). Adaptive maneuvering, with experiments, for a model ship in a marine control laboratory. *Autom.*, 41(2), 289 – 298.

Skjetne, R., Smogeli, Ø.N., and Fossen, T.I. (2004). A nonlinear ship manoeuvering model: Identification and adaptive control with experiments for a model ship. *Model. Identif. Control*, 25, 3–27.

Wang, N., Sun, Z., Yin, J., Zou, Z., and Su, S.F. (2019). Fuzzy unknown observer-based robust adaptive path following control of underactuated surface vehicles subject to multiple unknowns. *Ocean Eng.*, 176, 57 – 64.

Xia, Y., Xu, K., Li, Y., Xu, G., and Xiang, X. (2019). Improved line-of-sight trajectory tracking control of under-actuated AUV subjects to ocean currents and input saturation. *Ocean Eng.*, 174, 14 – 30.

Zhang, F., Marani, G., Smith, R.N., and Choi, H.T. (2015). Future trends in marine robotics. *IEEE Robot. Autom. Mag.*, 22(1), 14–122.

Zhao, Z.L. and Guo, B.Z. (2015). Extended state observer for uncertain lower triangular nonlinear systems. *Syst. Control Lett.*, 85, 100 – 108.